BUTTERWORTH HEINEMANN

Trajectories of burning coal particles in highly swirling reactive flows

J. Görres, U. Schnell and K. R. G. Hein
University of Stuttgart, Institut für Verfahrenstechnik und Dampfkesselwesen (IVD), Stuttgart, Germany

Finite-element computations and measurements of a strongly swirling flow with pulverized coal combustion are presented. The turbulent flow expands into a low confined combustion chamber which represents the geometry of typical industrial furnaces. Detailed in-flame measurements of velocity, temperature, and gas concentrations were made by suction probes at several cross sections. These data are used for the detailed evaluation of higher-order turbulence models in connection with coal combustion. In modeling the particle-gas flow, the momentum equations are solved by considering the particle phase as a continuum and neglecting the mean slip velocities between the two phases. Trajectories of the individual particles treated as inert matter are subsequently computed employing a Lagrangian method after a convergent flow field solution is obtained. The external forces which influence the particles' motion are considered and compared. Additionally, in a more realistic approach, the mass loss of the coal particles due to devolatilization and char-burnout is taken into account. The influence of the gas-phase turbulence modeling on the particle motion is also investigated.

Keywords: turbulence modeling; coal combustion; Lagrangian simulation

Introduction

Pulverized coal combustion can generally be characterized as a two-phase phenomenon: the heterogeneous coal particles are incorporated into a homogeneous gas-phase flow. In such combustion applications, a swirl component is usually imparted to the axial gas flow in order to achieve a stably burning flame or to influence the flame shape. In this context, an adequate modeling of the turbulent swirling flow is of utmost importance for obtaining reliable results, especially in predicting the near-burner zone, which is an important region for pollutant formation. In practical applications, a turbulence model serves to close the Favre or Reynolds-averaged governing equations by introducing modeled expressions for the Reynolds stresses in terms of known averaged quantities.

One of the most frequently employed turbulence models is still the standard k-ε model (Launder and Spalding 1974). However, the performance is often unsatisfactory in swirling flows (Srinivasan and Mongia 1980), since the strong anisotropic turbulence structures arising in flows with strong streamline curvature and rotation cannot be described adequately.

Due to the above-mentioned inadequacies in swirling flows, we have initiated an analysis of higher-order turbulence models using an algebraic stress model (ASM; Rodi 1976) for isothermal swirling flows (Görres et al. 1993a). Theoretically, the ASM provides a more accurate turbulence closure compared to the k-ϵ model, because the local values of the Reynolds stresses are not assumed to be proportional to the mean velocity gradients but are obtained directly by solving algebraic equations derived from the Reynolds stress transport equations.

These turbulence models are incorporated into an advanced finite-element code to compute turbulent fluid flow, reaction, and heat transfer in pulverized coal combustion. In deriving the discretization equations, a simplified streamline-upwind/Petrov–Galerkin method is employed, which has been found to be a suitable means to limit the effects of false diffusion (Görres 1995).

The investigation is extended to the prediction of particle motion in the turbulent swirling flow field. Along with that, a comparison is made about the magnitude of the resulting forces affecting the particles' motion due to the surrounding fluid flow. Further studies focus on the influence of the fluid turbulence model on particle motion and the consideration of the particles' mass loss due to combustion reactions.

Mathematical model

For statistically steady turbulent flows, the Favre-averaged Navier–Stokes equations can be expressed as

$$\frac{\partial}{\partial x_j}\left(\rho\overline{u_i}\overline{u_j}\right) = \frac{\partial}{\partial x_j}\left[\rho(1-\xi_P)\tau_{ij} - \frac{\partial}{\partial x_j}\left(\rho\overline{u_i'u_j'}\right)\right] - \frac{\partial p}{\partial x_i} \qquad (1)$$

with

$$\tau_{ij} = \mu_{\text{lam}}\left(\frac{\partial\overline{u_j}}{\partial x_i} + \frac{\partial\overline{u_i}}{\partial x_j}\right) - \frac{2}{3}\mu_{\text{lam}}\nabla\underline{u} \qquad (2)$$

For simplicity, overbars to indicate average quantities are dropped except for the velocities. ρ represents the density of the two-phase flow, and ξ_P the mass fraction of the particles. Along with the momentum equations, the continuity equation

$$\frac{\partial}{\partial x_j}\left(\rho\overline{u_j}\right) = 0 \qquad (3)$$

Address reprint requests to Dr. U. Schnell, Institut für Verfahrenstechnik und Dampfkesselwesen, University of Stuttgart, Pfaffenwaldring 23, D-70550, Stuttgart, Germany.

Received 20 January 1995; accepted 13 April 1995

Int. J. Heat and Fluid Flow 16: 440–450, 1995
© 1995 by Elsevier Science Inc.
655 Avenue of the Americas, New York, NY 10010

0142-727X/95/$10.00
SSDI 0142-727X(95)00046-S

is also solved. The task of a turbulence model is to find suitable approximations for the Reynolds stresses $\rho\overline{u_i'u_i'}$ in Equation 1. The predominantly used Boussinesq hypotheses (Launder and Spalding 1974) closes the averaged Navier–Stokes Equation 1 by relating the Reynolds stresses to local mean quantities by introducing a scalar variable called turbulent viscosity μ_t

$$\rho\overline{u_i'u_j'} = \frac{2}{3}[\mu_t \nabla \underline{u} + \rho k]\delta_{ij} - \mu_t\left(\frac{\partial \overline{u_i}}{\partial x_j} + \frac{\partial \overline{u_j}}{\partial x_i}\right) \tag{4}$$

Applying the k-ε model, the turbulent viscosity for the two-phase flow is modeled by

$$\mu_t = \rho C_\mu \frac{k^2}{\varepsilon}(1-\xi_P)^{0.5}\left[(1-\xi_P) + \xi_P\left(1+\frac{t_R}{t_E}\right)^{-1}\right] \tag{5}$$

In Equation 5, the particle phase is taken into account by two additional terms (Görres 1995). The ratio of the relaxation time and the eddy dissipation time of the gas phase is given by

$$\frac{t_R}{t_E} = \frac{\rho_P d_P^2}{18\mu_{\text{lam}}}\frac{\sqrt{2}}{C_\mu^{0.75}}\frac{\varepsilon}{k} \tag{6}$$

k and ε represent the kinetic energy of turbulence and its dissipation rate, respectively; whereas $C_\mu = 0.09$ is a model constant. For both turbulence quantities, additional transport equations are solved (Görres et al. 1993a).

An advanced approach for closing Equation 1 is the ASM first proposed by Rodi (1976). Here, the Reynolds stresses are obtained by solving algebraic equations

$$\rho\overline{u_i'u_j'} = \frac{2}{3}\rho k\delta_{ij} + \gamma\frac{k}{\varepsilon}\left(P_{ij} - \frac{2}{3}P\delta_{ij}\right) \tag{7}$$

with the variable

$$\gamma = \frac{1-C_2}{C_1 - 1 + P/\varepsilon} \tag{8}$$

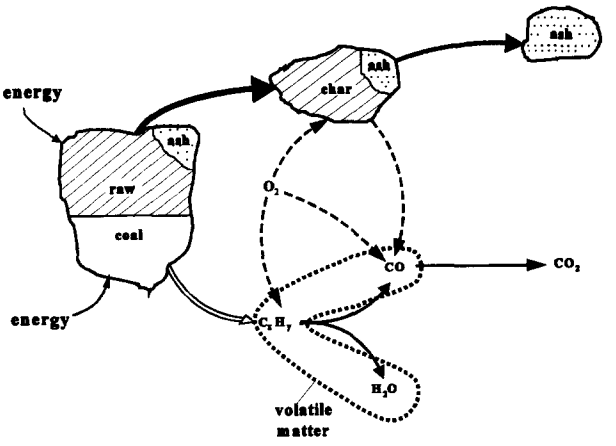

Figure 1 Reaction model of pulverized coal combustion

and the model constants $C_1 = 2.5$ and $C_2 = 0.55$. P_{ij} is the production rate of turbulence, modeled as

$$P_{ij} = -\rho\left(\overline{u_i'u_k'}\frac{\partial \overline{u_j}}{\partial x_k} + \overline{u_j'u_k'}\frac{\partial \overline{u_i}}{\partial x_k}\right) \tag{9}$$

and with P (cf. Equation 7) $= 0.5\ P_{ii}$.

Apart from the conservation of momentum, the transport of mass and energy must be modeled. For the gas-phase concentration of a species α, the transport equation can be expressed as

$$\rho\overline{u_j}\frac{\partial \xi_{G,\alpha}}{\partial x_j} = \frac{\partial}{\partial x_j}\left[\left(\frac{\mu_{t,0}(1-\xi_P)^{0.5} + (1-\xi_P)\mu_{\text{lam}}}{\sigma_{G,\alpha}}\right)\frac{\partial \xi_{G,\alpha}}{\partial x_j}\right] + S_{G,\alpha} \tag{10}$$

Notation

c_P	specific heat capacity, kJ/(kg K)
C	constant
d	diameter, m
F	force, N
g	gravitational acceleration, m/s^2
h	specific enthalpy, kJ/kg
k	kinetic energy of turbulence, m^2/s^2
k	frequency factor of reaction, 1/s
P	turbulent kinetic energy production, kg/(m s^3)
p	pressure, bar
Re	Reynolds number
r	radial direction or position, m
T	temperature, K
t	time, s
u	velocity, m/s
x	coordinate, m
z	axial position, m

Greek

α	species index
δ_{ij}	Kronecker delta
ε	Dissipation rate of turbulent energy, m^2/s^3
η	random variable
λ	thermal conductivity, kW/(m K)
μ	dynamic viscosity, kg/(m s)
ξ	mass fraction
ρ	density kg/m^3
σ	Prandtl/Schmidt number
τ	shear stress, N/m^2

Superscripts

$'$	fluctuating
$-$	mean value (Favre averaging)

Subscripts

e	eddy
G	gas phase
i, j	indices
lam	laminar
P	particle
rad	radiation
RK	raw coal
S	solid
t	turbulent
VM	volatile matter

with $\sigma_{G,\alpha} = 0.7$. $S_{G,\alpha}$ is termed the local source of $\xi_{G,a}$ per unit mass and accommodates the source and sink terms due to species conversion modeled by an appropriate reaction model (see below).

The energy transport is described by the conservation of total specific enthalpy

$$\rho\overline{u_j}\frac{\partial h}{\partial x_j} = \frac{\partial}{\partial x_j}\left(\frac{(\mu_{\text{lam}} + \mu_t)}{\sigma_h}\frac{\partial h}{\partial x_j}\right) + S_h \tag{11}$$

with

$$\sigma_h = \frac{\mu_{\text{lam}} c_p}{\lambda} \tag{12}$$

computed from the specific heat capacity c_P and the thermal conductivity λ of the gas phase. Since the heat release due to the chemical reaction is implicitly incorporated when the *total* energy is balanced, the source term S_h comprises radiative heat transfer which is modeled by a momentum radiation model for the particle laden flow (Görres 1995).

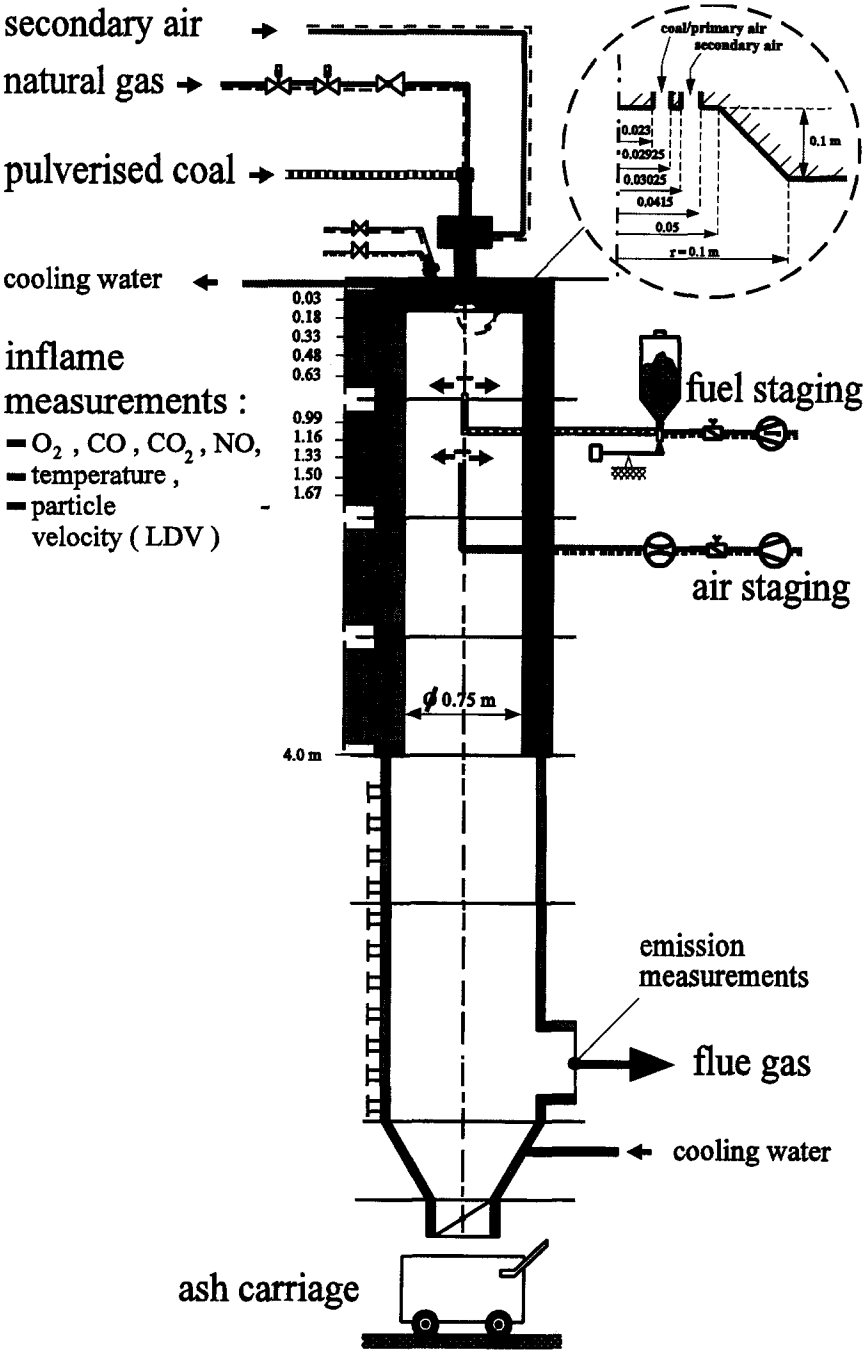

Figure 2 Semi-industrial coal combustion facility, 350 MW_{th}

Modeling pulverized coal combustion necessitates an approach for the description of the motion of the particle phase. If the conservation equation for a particle concentration $\xi_{P,\alpha}$ is formulated equivalent to the transport of a conserved variable, e.g., enthalpy (Equation 11), an Eulerian form is yielded

$$\rho\bar{u}_j\frac{\partial\xi_{P,\alpha}}{\partial x_j}=\frac{\partial}{\partial x_j}\left[\frac{\mu_{t,0}(1-\xi_P)^{0.5}}{\sigma_{P,\alpha}}\left(1+\frac{t_R}{t_E}\right)^{-1}\frac{\partial\xi_{P,\alpha}}{\partial x_j}\right]+S_{P,\alpha} \tag{13}$$

with $\sigma_{P,\alpha}=0.7$ and $\xi_P=\Sigma\xi_{P,\alpha}$. $\mu_{t,0}$ (cf. Equations 10 and 13) characterizes the dynamic viscosity of the gas phase without all terms in brackets in Equation 5. The source terms $S_{P,\alpha}$ depend on the modeling assumptions for the description of pulverized coal combustion.

In deriving Equation 13, it has been assumed that complete mathematical modeling of all terms appearing in the averaged equation is beyond the necessities for the present purposes. Therefore, a proposal of Melville and Bray (1979) for modeling turbulent particle diffusion has been extended and applied to model the term $\rho\overline{u_i'\xi_{P,\alpha}'}$ thus yielding the expression in brackets in Equation 13. Further simplifications are obtained by assuming that mean particle slip velocities can be neglected, thus allowing us to determine only one velocity vector representative for the mean motion of the two-phase flow. This assumption seems to be

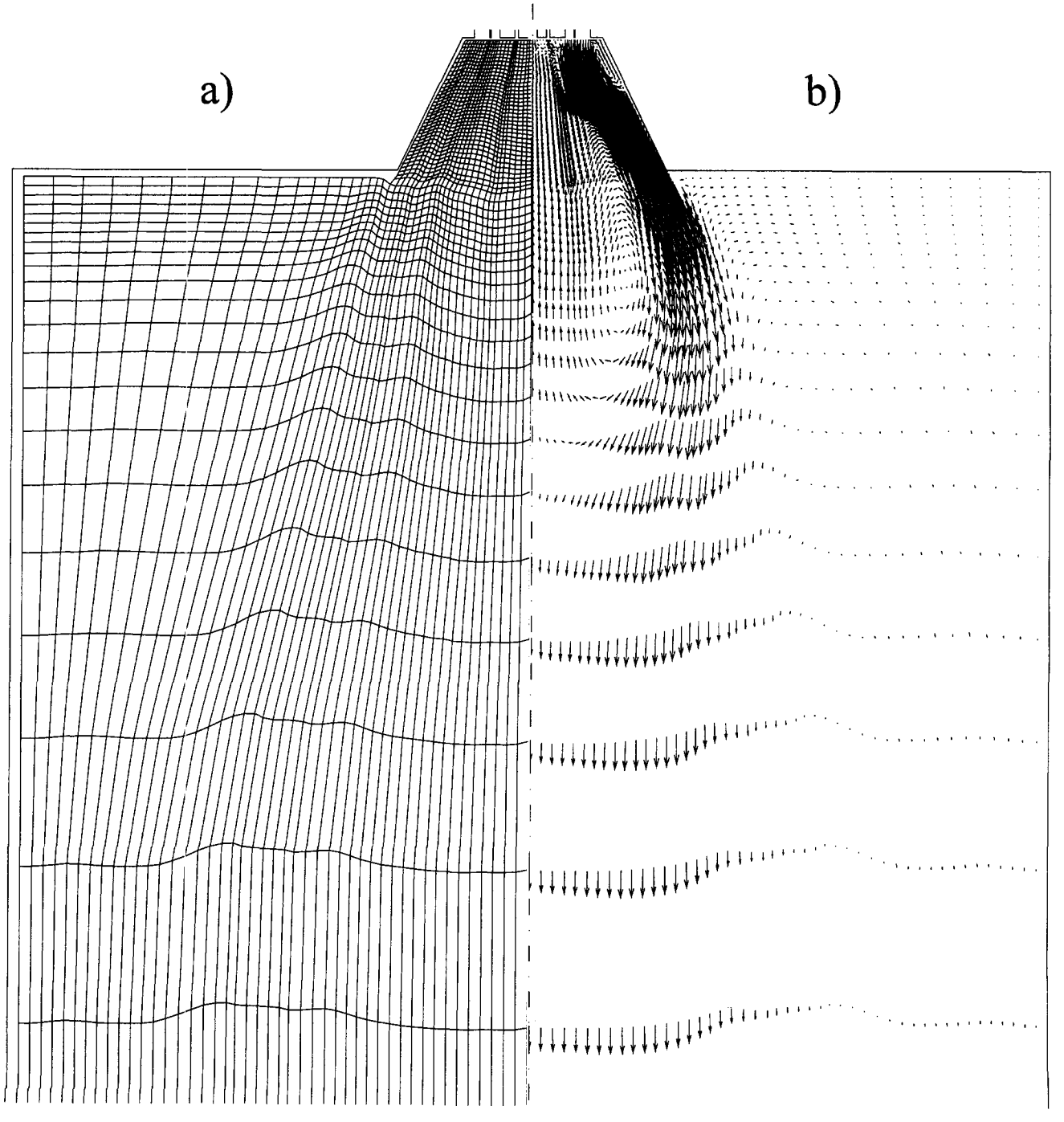

justified in two-phase flows with very low mass loadings (Sommerfeld and Qui 1993) as it is typical for the investigated case.

The modeled reaction scheme of pulverized coal combustion assumes four reaction steps (Figure 1). In the first step, the coal is devolatized yielding volatile matter (C_xH_y, CO, H_2O) and char. Char oxidation to CO is the second reaction step, which is limited by the kinetic reaction rate and the diffusion rate of oxygen to the particle surface. The governing volatile species C_xH_y is oxidized to H_2O and CO, assuming that the reaction progress is limited by eddy mixing. The oxidation of CO to CO_2 is modeled using an eddy-mixing approach, as well. The effect of

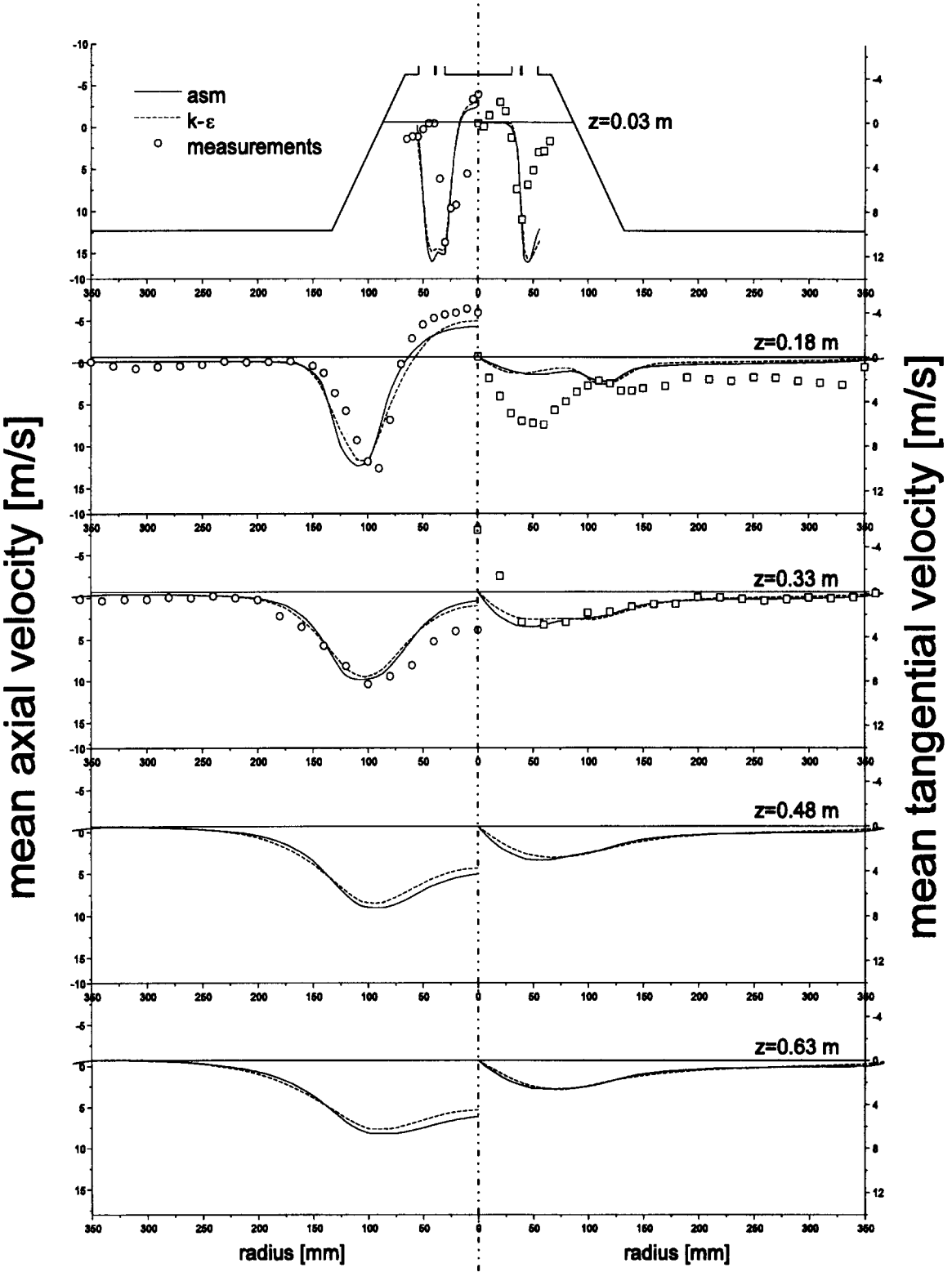

Figure 4 Mean axial and tangential velocity

the coal particle size distribution on reaction rates is considered by assuming six distinct particle size classes. Thus, the particle transport Equation 13 is solved for the mass fractions of coal and six char particle sizes. A more detailed description of the coal combustion model is presented by Schnell et al. (1993).

To study the motion of individual coal particles in more detail, a supplementary investigation has been initiated. It is based on the assumption that the flow field obtained by the solution of the transport equations formulated in the Eulerian framework is not altered by the particle movement. Thus, if

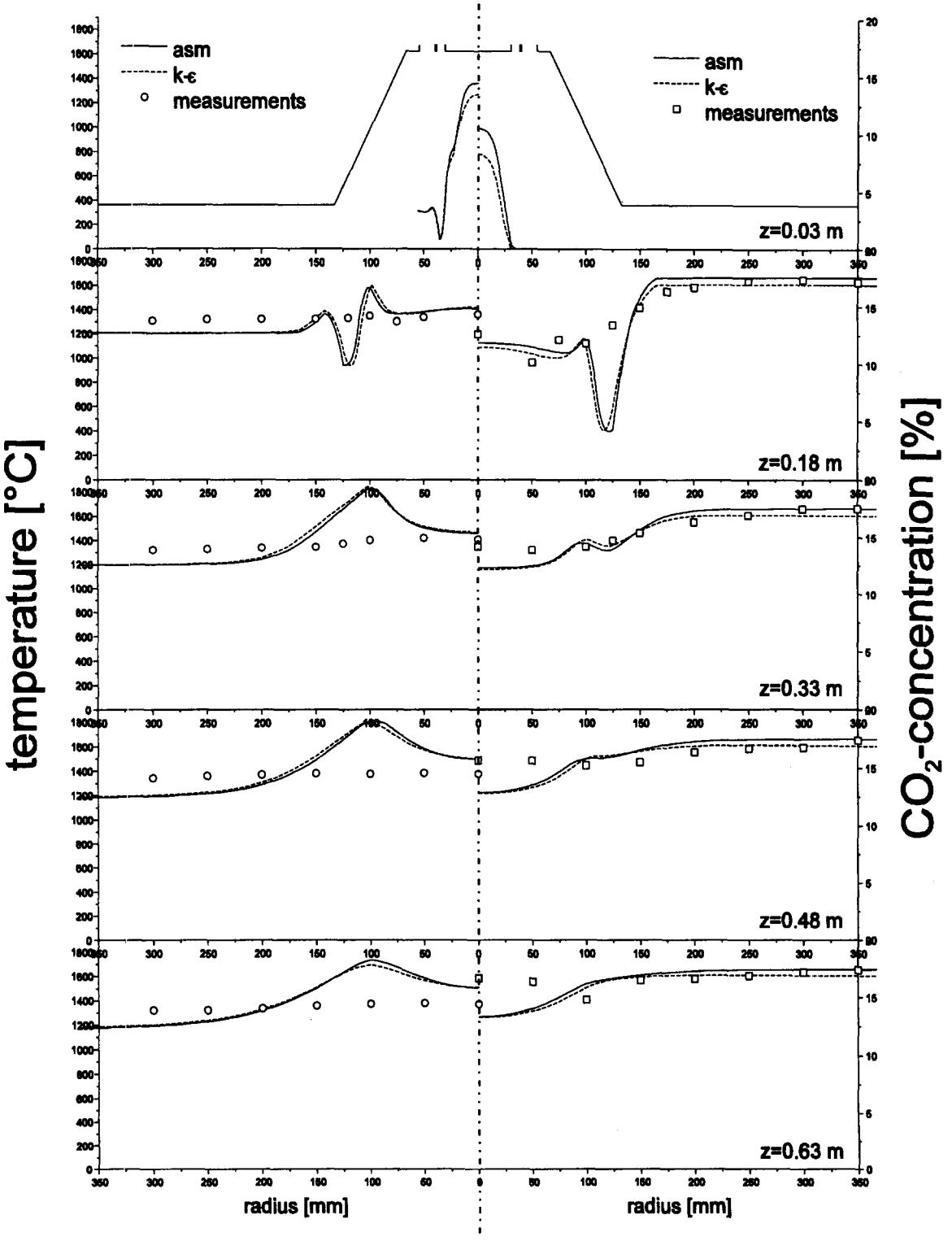

Figure 5 Temperature and CO_2 concentration

particle–particle interactions are neglected, the particle trajectories can be determined in a Lagrangian frame of reference (Boysan et al. 1982)

$$\frac{\partial}{\partial t}(m_p\, u_{P_i}) = F_W + F_G + F_{VM} + F_C + F_A + F_S + F_M + F_B \quad (14)$$

The motion of an individual particle is influenced by several external forces: the drag force F_W, the apparent external mass force F_G, the virtual mass force F_{VM}, the centrifugal and the coriolis force F_C, which appear in a cylindrical coordinate system, the buoyancy force F_A, the Saffman force F_S, the Magnus force F_M, and the Basset history force F_B. In the following section, the magnitude of these forces is compared, and it is shown that only F_W, F_G, and F_S have to be considered when modeling coal particle motion. In this case, Equation 14 can be rewritten as

$$\frac{\partial u_{P_i}}{\partial t} = \frac{1}{t_R}\left\{(\bar{u}_i + u_i') - u_{P_i}\right\} + g_i + C_S d_P^2 (\mu_{lam}\rho)^{0.5}\left\{(\bar{u}_i + u_i') - u_{P_i}\right\}\frac{\partial \bar{u}_j}{\partial x_i} - \frac{u_{P_i}}{m_P}\frac{\partial m_P}{\partial t} + F_C \quad (15)$$

with the Saffman constant $C_S = 1.61$. t_R represents the particle relaxation time which can be given as

$$t_R = \frac{\rho_P d_P^2}{18\mu_{lam}\left(1 + 0.15\ \mathrm{Re}_P^{0.687}\right)} \quad (16)$$

It is assumed that the mean velocity of the two-phase flow previously determined by the solution of the Eulerian transport equations may be identified with the mean gas-phase velocity $\bar{u}_i$ in Equation (15). The fluctuating gas phase velocities u_i' are modeled, using a stochastic approach, as

$$u_i' = \eta\sqrt{\overline{u_i' u_i'}} \quad (17)$$

where η denotes a normally distributed random variable. The Reynolds stress tensor components $\overline{u_i' u_i'}$ are provided either by the k-ε model assuming a standard deviation

$$\overline{u_i' u_i'} = (2/3)k \quad (18)$$

or by the ASM according to Equation 7.

The interaction time of the particle with an eddy is the minimum of the eddy lifetime

$$t_{e1} = \frac{C_\mu^{3/4}}{\sqrt{2}}\frac{k}{\epsilon} \quad (19)$$

and the time that a particle needs to cross an eddy is

$$t_{e2} = \frac{\sqrt{\overline{u_i' u_i'}}\cdot t_{e1}}{\sqrt{\left(\bar{u}_i - u_{P_i}\right)^2}} \quad (20)$$

If the Lagrangian treatment of the particle motion presented so far is extended to reacting particles, the mass loss due to devolatilization and char burnout

$$\frac{\partial m_P}{\partial t} = -k_P \cdot m_P \quad (21)$$

has to be included (cf. Equation 15). The coal weight loss during pyrolysis is estimated using a single-step reaction with an Arrhenius-type expression. The char burnout is controlled by the diffusion rate of oxygen to the particle surface and by the kinetic

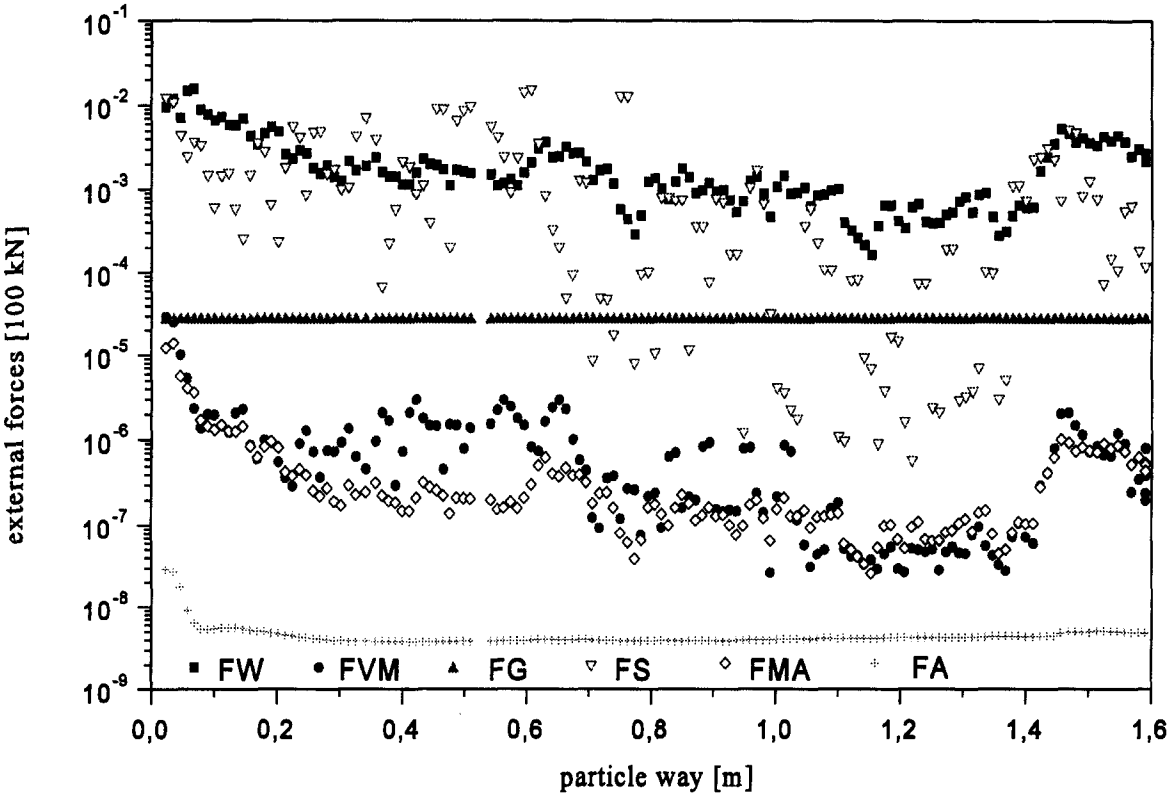

Figure 6 External forces affecting the motion of inert particles, $d_p = 33.5$ μm

rate of carbon oxidation. The mechanism is described in detail by Görres (1995).

The equations of particle motion can be integrated analytically assuming sufficiently small time increments in which the gas velocities and body-force terms remain constant (Benim 1990). Beginning from the starting location in the burner inlet, the particle location along its trajectory through the furnace is determined from

$$\frac{\partial x_{P_i}}{\partial t} = u_{P_i} \tag{22}$$

Numerical computations

To validate the proposed mathematical model of pulverized coal combustion, data obtained at our semi-industrial coal combustion facility (Maier et al. 1991) are used. The diameter and length of the vertical combustion chamber are 0.75 m and 7 m, respectively. The burner quarl has an angle of about 25° and a length of 0.1 m. This geometry represents a typical example of a burner flow into a low confinement (Figure 2).

The pulverized coal (35 kg/h) is transported with air (56 m^3_N/h, 60°C) through the primary inlet with no tangential momentum. One part of the combustion air (140.7 m^3_N/h, 280°C) with a swirl number of 0.85 enters the furnace through the secondary inlet, the other part (147.2 m^3_N/h, 280°C) through a lance at an axial distance of 1.38 m from the burner. The mean axial velocities are 20 m/s in the primary inlet and 32 m/s in the secondary inlet. Thus, the particle mass concentration is very low with its maximum value of 0.1354 in a small region in the vicinity of the primary inlet.

Figure 3a shows the finite-element mesh ($0 \leqslant z \leqslant 0.7$ m), with 2,929 nodes and 2,816 elements. To get a grid-independent solution, a self-adapting grid scheme is used (Nakahashi and Diewert 1986). The number of nodes is kept constant, while the grid is moved dependent on the local velocity gradients. In the burner quarl, the elements are adapted to the high-velocity gradients of the secondary air in the near-wall region.

The computed velocities in axial and radial direction are shown in Figure 3b. Due to the swirl, the flow in the burner quarl is pushed to the wall, thus establishing an internal recirculation zone (IRZ). Compared to an unstaged flame presented by Görres et al. (1993b), the size of the IRZ is reduced, because the amount of swirled combustion air is lowered to a stoichiometric ratio of 0.7 in the primary zone.

In the following, the simulation results of the finite-element computation are compared with experimental data at several axial distances from the burner. Velocity measurements were carried out by applying the laser-Doppler-velocimetry (LDV) technique. Temperature and gas concentrations (O_2, CO_2, CO, NO_x) were measured at several cross sections using suction probes.

The computed axial and tangential velocities for the k-ε model and the ASM are plotted *versus* the distance from the centerline in Figure 4. The numerical results show good agreement with measured data of axial velocity. There are only small differences between both turbulence models for this test case. Using the ASM, the steep gradient at $z = 0.18$ m, $r = 75$ mm is better predicted than with the k-ε model. For the tangential velocity, both turbulence models cannot adequately reproduce the qualitative shape of the experimentally determined curve at $z = 0.18$ m. However, at $z = 0.33$ m, the ASM results are slightly closer to the measurements. Further downstream, the flow field is homogenized, and the swirl component vanishes. The temperature profile and the mass concentrations of CO_2 are shown in Figure 5.

The k-ε and ASM model predictions show more structure throughout the furnace than the measured values. In the predicted temperature profiles, the influx of cold secondary air is still visible at $z = 0.18$ m. This phenomenon cannot be detected in the temperature data. It has been frequently reported that measurements of very steep temperature gradients by suction pyrometer are subject to errors (Weber et al. 1992). The agreement of computation and CO_2 measurements is quite good, although the spatial resolution of the experimental data is too coarse.

In the predictions presented so far, the Eulerian formulation of the transport equations (Equations 1–13) has been used. For the following investigation of the motion of particles in swirling pulverized coal flames, the Lagrangian treatment according to Equations 14–22 is applied. In Figure 6, the forces which influence the particles on their way through the furnace are compared for an inert particle with a diameter of $d_p = 33.5$ μm.

The values of the external forces differ significantly, the drag force F_W being predominant. The Saffman force F_S is very important if high-velocity gradients appear. In this example, F_S

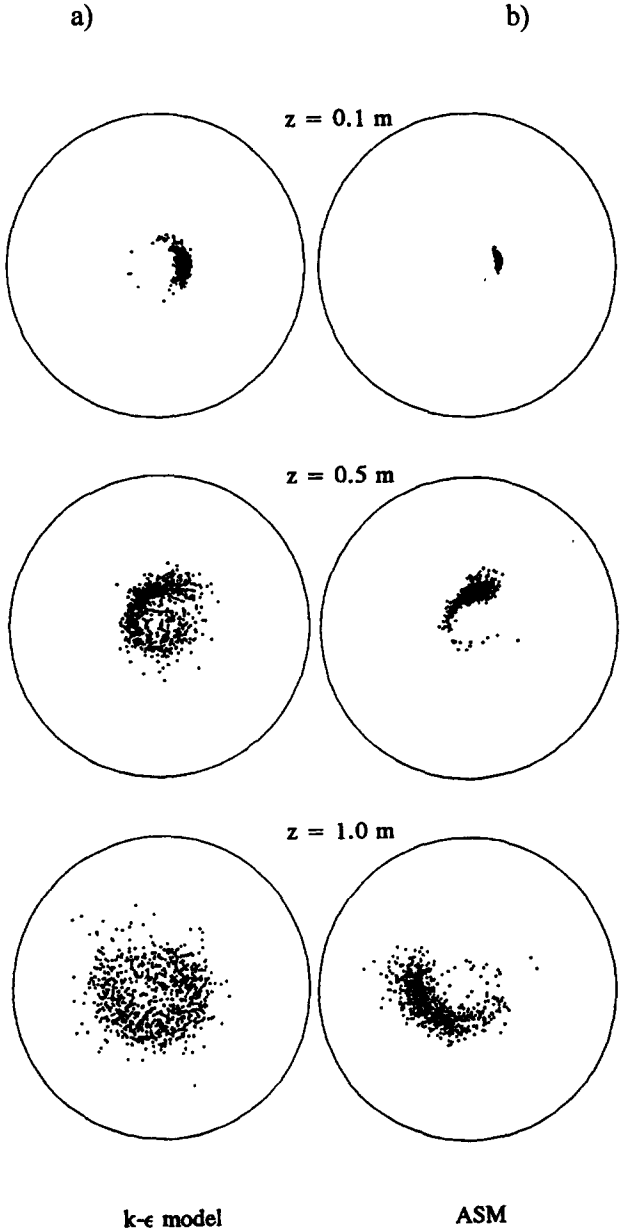

Figure 7 Piercing points of inert particles at several cross sections

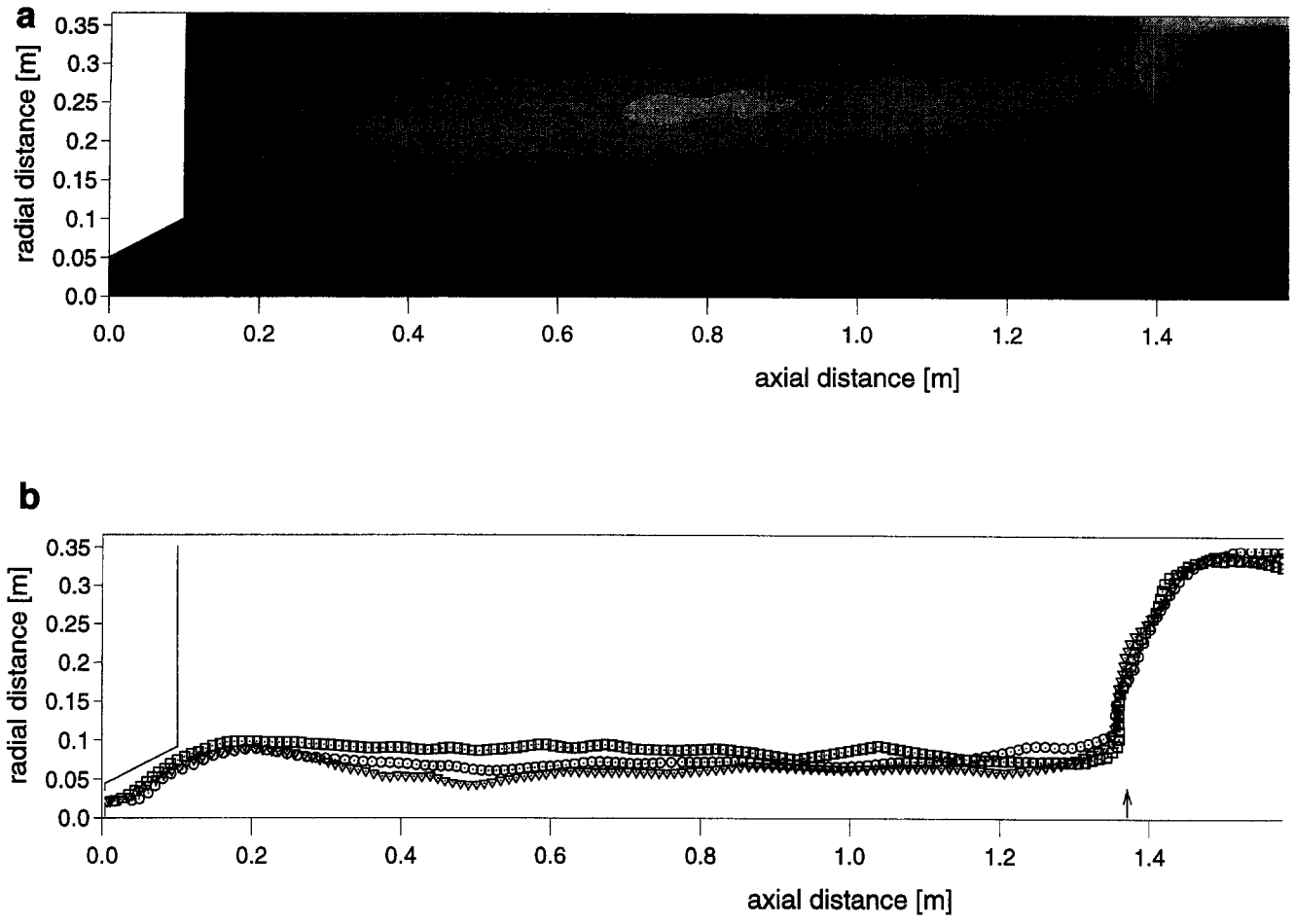

Figure 8 Trajectories of inert particles: a) streamlines (% of total inlet mass flow); b) particle trajectories, □ $d_p = 8.0$ μm, ▽ $d_p = 33.5$ μm, ○ $d_p = 59.0$ μm

has the same order of magnitude as the drag force. Only at the end of the particle track, where lower gas phase velocity gradients prevail, is F_S reduced by two orders of magnitude. The external mass force F_G is constant for this nonreacting particle. The virtual mass force F_{VM}, which describes the influence of the acceleration of the particle if the gas is accelerated, the Magnus force F_M, and the buoyancy force F_A can be neglected. Since the ratio of particle density to gas density is in the range of 1000, the Basset history force F_B is also negligible.

To investigate the effect of gas-phase turbulence modeling on particle dispersion, particle trajectories are computed based on two different flow field solutions computed with the Eulerian treatment; a k-ε model prediction and an ASM result. In both studies, 1000 particles are injected at the same location in the burner. In Figure 7, the piercing points of the particles through several cross sections are plotted.

The figure shows how the particle "cloud" rotates due to the swirling gas motion. At the same time, it is dispersed by turbulent movements as it proceeds in the axial direction. Inspecting the distribution of the piercing points, it can be observed that a higher degree of turbulent particle dispersion is predicted when a k-ε model for the gas flow is used instead of an ASM. This observation corresponds with the higher kinetic energy predicted by the k-ε model on the order of 15%.

In Figure 8, the streamlines of the pulverized coal flame (cf. Figure 3) computed with the Eulerian approach and using an ASM are compared with the mean trajectories of inert particles with three different diameters. The particle paths are the average of five trajectories. Thus, the stochastic effects caused by the gas-phase turbulence are not visible in this graph.

It may be concluded that the particles with the smallest diameter ($d_p = 8$ μm) follow the streamlines of the gas flow (Figure 8a) without any slip. The particles with medium diameter ($d_p = 33.5$ μm) and particularly the biggest particles ($d_p = 59.0$ μm) penetrate the IRZ. All particles are entrained into the air-staging flow at $z = 1.38$ m and are subsequently pushed toward the furnace wall.

In Figure 9a, the weight loss of reacting coal particles due to devolatilization is taken into account. The particle trajectories are computed until the volatile matter is completely evolved. Only the biggest particles enter the IRZ, where devolatilization is completed very rapidly. The smallest particles are entrained into the secondary air and undergo devolatilization at the end of the burner quarl.

In a further study, the mass loss of the particles due to the burnout of the char was additionally considered (Figure 9b). The computed trajectories give further evidence that the burnout of the small particles takes place along the outer boundary of the IRZ.

Conclusions

Numerical computations of a reacting swirling flow in a semi-industrial pulverized coal combustion facility were reported. A higher-order turbulence model (ASM) which was incorporated

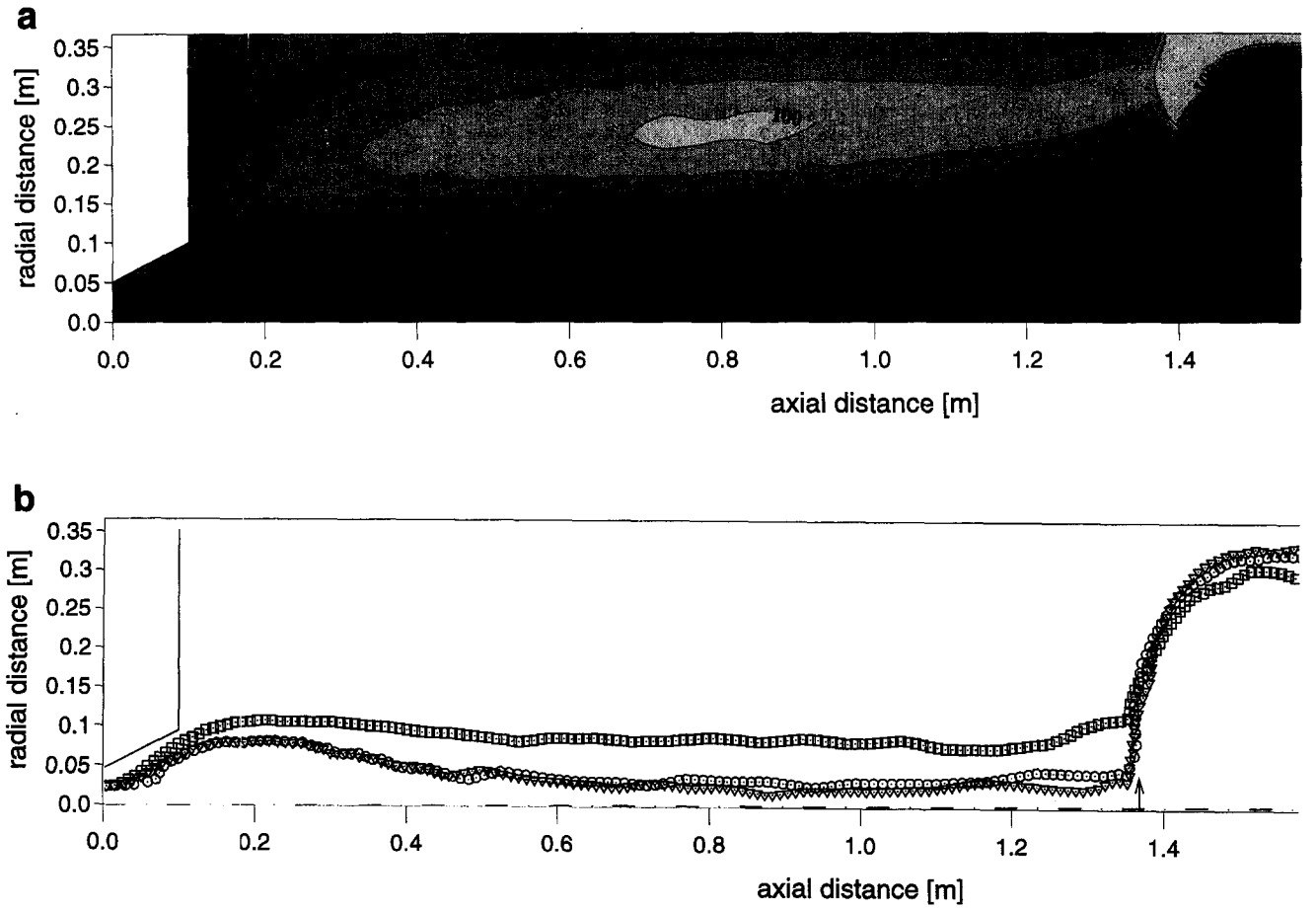

Figure 9 Trajectories of reacting coal particles: a) only pyrolysis; b) complete burnout; □ d_p = 8.0 μm, ▽ d_p = 33.5 μm, ○ d_p = 59.0 μm

into a finite-element code was compared with k-ε model predictions and with measurements. Only small improvements were accomplished using the ASM for the coal flame under investigation.

A numerical study on the magnitude of external forces affecting the particle motion in the turbulent flow field showed that only a few forces are of importance for the particle trajectory. Most of the particles with small and medium diameter are able to follow the motion of the gas flow without slip. Taking devolatilization into account, even the bigger particles have lost the bulk of their initial mass at the end of the burner quarl. Due to the subsequent burnout of the remaining char particles, the velocity difference between gas and particle phase decreases continuously. Thus, the critical assumption that particles can be treated as a continuum in the coal combustion process seems to be justified for most of the furnace domain in the case under investigation.

Acknowledgments

This work was carried out within the TECFLAM project on Mathematical Modeling and Laser Diagnostics of Combustion Processes. Funding by the German Ministry of Research and Technology and the Federal Government of Baden-Württemberg is gratefully acknowledged.

References

Benim, A. C. 1990. Finite element analysis of confined turbulent swirling flows. *Int. J. Num. Methods Eng.*, **11**, 697–717

Boysan, F., Ayers, W. H. and Swithenbank, J. 1982. A fundamental mathematical modeling approach to cyclone design. *Trans. IChemE*, **60**, 222–230

Görres, J. 1995. Modellierung stark verdrallter Kohlenstaub/Biomasse flammen mit der Methode der Finiten Elemente. Ph. D. thesis, University of Stuttgart, to be published as "VDI-Fortschritts-Bericht" (in German)

Görres, J., Fingerle, A., Magel, H. C. and Schnell, U. 1993a. Finite element analysis of turbulence models for confined swirling flows using LDV-measurements for verification. In *Computational Methods Experimental Measurements VI*, C. A. Brebbia and G. M. Carlomagno (eds.), Comp. Mech. Publ., Vol. 1: *Heat and Fluid Flow*, 337–352

Görres, J., Benim, A. C., Magel, H. C.; Schnell, U. 1993b. Finite element analysis of turbulence models for confined swirling flows with combustion. In *Finite Elements in Fluids: New Trends and Applications*, Part I, K. Morgan, E. Oñate, J. Périaux, J. Peraire and O. C. Zienkiewicz (eds.), Pineridge Press, Barcelona, 469–478

Launder, B. E. and Spalding, D. B. 1974. The numerical computation of turbulent flows. *Comp. Appl. Mech. Eng.*, **3**, 269–289

Maier, H., Brodbek, H., Kaess, M., Kicherer, A. and Spiegelhalder, R. 1991. Investigations in staged coal combustion with regard to mixing properties carried out at a semi-industrial test facility. *Proc. 2nd International Symposium on Coal Combustion Science and Technology*, China, 567–577

Melville, W. K. and Bray, K. N. C. 1979. A model of the two-phase turbulent jet. *Int. J. Heat Mass Transfer*, **22**, 647–656

Nakahashi, K. and Deiwert, G. S. 1986. Three-dimensional adaptive grid method. *AIAA J.*, **24**, 948–954

Rodi, W. 1976. A new algebraic relation for calculating the reynolds stresses. *Zeitschr. f. angew. Math. Mech. (ZAMM)*, **56**, T219–T221

Schnell, U., Kaess, M. and Brodbek, H. 1993. Experimental and numerical investigation of NO_x formation and its basic interdependencies on pulverized coal flame characteristics. *Combustion Sci. and Tech.*, **93**, 91–109

Sommerfeld, M. and Qiu, H.-H., 1993. Characterization of particle-laden, confined swirling flows by phase-Doppler anemometry and numerical calculation. *Int. J. Multiphase Flow*, **19**, 1093–1127

Srinivasan, R. and Mongia, H. C. 1980. Numerical computation of swirling recirculating flows. Final Report, NASA CR-165196

Weber, R., Dugué, J., Sayre, A., Peters, A. and Visser, B. M., 1992. Measurements and computations of quarl zone flow field and chemistry in a swirling pulverized coal flame. IFRF Doc. F 36/y/20.